OPEN ACCESS

Applied Physics Express **16**, 102002 (2023)

LETTER

https://doi.org/10.35848/1882-0786/acfe59

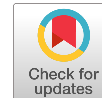

Nonlinear propagation calculation-based irradiation process control for several mJ ultrashort pulse laser processing

Itsuki Nishibata* and Tomokazu Sano

Division of Materials and Manufacturing Science, Graduate School of Engineering, Osaka University, Suita, Osaka, 565-0871, Japan

*E-mail: i.nishibata@mapse.eng.osaka-u.ac.jp

Received July 28, 2023; revised September 4, 2023; accepted September 27, 2023; published online October 12, 2023

In the realm of ultrashort pulse laser processing, surpassing the air ionization threshold, variations in focusing characteristics due to nonlinear optical phenomena pose challenges. Particularly, suitable irradiation conditions and position control methods for high pulse energy processing around 1 mJ remain unestablished. This study explores laser divergence phenomena in several mJ pulse energy range, examining both experimental and computational data. Quantitative demonstrations of laser focusing alterations, including divergence position and fluence, were achieved. Additionally, the dry laser peening effect was enhanced by energy-specific irradiation control. Numerical simulation-based visualization facilitates precise control, advancing the processing techniques. © 2023 The Author(s). Published on behalf of The Japan Society of Applied Physics by IOP Publishing Ltd

Supplementary material for this article is available online

Ultrashort pulse lasers facilitate precise material removal with negligible thermal effects, employing pulse energies in the order of tens of μJ.[1,2] Moreover, higher pulse laser energy enables the exploitation of laser impact force.[3] Dry laser peening, harnessing this impact force, enhances material properties, including residual stress, hardness, fatigue, and corrosion resistance.[4–6] Unlike the mainstream nanosecond laser peening using water, ultrashort pulse lasers offer the advantage of air-based application, albeit with a relatively shallow peening effect.[7] In dry laser peening, superior peening effects are achieved with several hundred μJ compared to pulse energy conditions of several tens of μJ,[4] and the process is expected to utilize higher pulse energy.

However, the focusing characteristics of ultrashort pulse lasers at high pulse energies are influenced by nonlinear optical phenomena in the air, leading to changes.[8,9] A profound understanding of these focusing characteristics is imperative, as laser intensity and fluence distribution during irradiation significantly impact laser processing features.[10,11] Visualizing high-intensity lasers directly using cameras is infeasible, necessitating simulations based on nonlinear propagation calculations.[12–14] Although numerous studies focus on laser filamentation with focal lengths on the order of meters, there are limited examples of nonlinear propagation calculations within the realm of ultrashort pulse laser processing. To the best of our knowledge, there exists a solitary investigation comparing nonlinear propagation calculations and processing outcomes in the mJ energy domain, specifically limited to the 1 mJ condition. This study solely contrasts processing experiments and calculated fluence distributions exclusively at the focal point.[15] Although a handful of reports address processing and calculations at pulse energies below 200 μJ, their scope remains confined to the examination of fluence distribution exclusively at the focal point and resultant processing outcomes.[16–18] In the context of mJ-class pulse energy focusing, the influence of nonlinear optical phenomena within the atmosphere assumes significance, thereby rendering focal point processing not universally suitable. Consequently, the exploration of alterations in focusing characteristics, including upstream divergence phenomena from the focal point, emerges as a requisite discussion. However, no prior research has centered on scrutinizing fluence distribution and processing outcomes at positions preceding the focal point along the propagation direction. Of particular significance is the comprehensive investigation of laser focusing variations and corresponding processing attributes across an array of pulse energies, encompassing sub-mJ to several mJ, to establish their utility in ablation and laser shock processing.

In this study, we explored the focusing characteristics of ultrashort pulse lasers and the pulse energy dependency of the dry laser peening effect in the energy range of 0.1–3.0 mJ. To this end, we performed nonlinear propagation calculations near the focal point and conducted ablation processing experiments at each energy level, evaluating the fluence distribution around the focus. Utilizing the acquired data, we meticulously controlled the irradiation position during laser peening, measured the imparted amount of compressive residual stress—representative of peening effects—and evaluated the pulse energy's influence. This study furnishes fundamental insights essential for the widespread, universal, and efficient implementation of high-energy ultrashort pulse laser processing.

First, we present the nonlinear propagation calculation method using the following laser parameters: 800 nm wavelength, 5 mm beam radius, 100 fs pulse duration (full-width at half maximum), and three pulse energy levels—0.1 mJ, 1.0 mJ, and 3.0 mJ. Focusing was achieved with a plano-convex lens of 250 mm focal length. The M2 of the laser beam is less than 1.1 and was ignored in the numerical calculations. The nonlinear propagation calculations were performed using the numerical Schrödinger equation, along with numerical computation of the electron rate equation, which are standard techniques in the field of nonlinear propagation calculations.[13] See the supplementary data for the meaning of symbols used in the formula

Content from this work may be used under the terms of the Creative Commons Attribution 4.0 license. Any further distribution of this work must maintain attribution to the author(s) and the title of the work, journal citation and DOI.

© 2023 The Author(s). Published on behalf of The Japan Society of Applied Physics by IOP Publishing Ltd

$$\frac{\partial \mathcal{E}}{\partial \xi} = \frac{i}{2k_0}\Delta_\perp \mathcal{E} - i\frac{k_0^{(2)}}{2}\frac{\partial^2 \mathcal{E}}{\partial \tau^2} + i\frac{k_0}{n_0}n_2 I \mathcal{E} - \frac{1}{2}\frac{W(I)K\hbar\omega_0(\rho_{nt}-\rho)}{I}\mathcal{E} - \frac{\sigma_{IB}(\omega_0)}{2}(1+i\omega_0\tau_c)\rho\mathcal{E} \quad (1)$$

$$\frac{d\rho}{dt} = W(I)(\rho_{nt}-\rho). \quad (2)$$

In Eq. (1), $\mathcal{E}$ represents the envelope of the complex electric field amplitude of the normalized laser pulse. The right-hand side of the equation consists of several terms with specific physical meanings. The first term accounts for diffraction, the second term corresponds to dispersion, while the third and subsequent terms encompass various nonlinear optical effects. Among these terms, the third one represents the Kerr effect, the fourth one denotes absorption due to ionization of the laser field, and the fifth term captures both plasma absorption in the real part and plasma defocusing in the imaginary part. Various pertinent parameters for the calculations can be found in Table I. Equation (2), regarding the electron rate equation, it comprises essential components such as laser ionization, impact ionization, and recombination. However, in this particular calculation, the effects of impact ionization and recombination were neglected due to their minimal influence on pulse durations of approximately 100 fs.[19,20] The PPT model was employed to determine the laser intensity-dependent ionization rates.[12,21,22] Refer to the supplementary data for detailed methods of ionization rate calculations.

Next, the transition of spot area (strong ablation area) in the direction of propagation is evaluated experimentally. Al alloy 2024-T351 was used as the specimen material in this experiment; the composition of Al2024-T351 is shown in Table II. To investigate the spot area near the focal point, as illustrated in Fig. 1(a), an *xyz* stage was employed to subject the specimen to 8 laser pulses, ranging from 10 mm upstream to 5 mm downstream from the focal position in a linear propagation regime. The focal position in a linear propagation regime was ascertained by focalizing the laser with a pulse energy of 20 μJ. In this condition, the irradiation area was most focused at a specific point and exhibited symmetry around that point, therefore designating that point as the focal position in a linear propagation regime. A typical irradiation mark comprises both the spot area and the irradiation area (weak ablation area), as depicted in Fig. 1(b). The spot area was defined as the region where 2.5 μm was removed per 8 shots, and its measurement was carried out using a laser microscope (VK-9700, Keyence Corp.). During dry laser peening, irradiation is applied while scanning the entire surface layer, as shown in Fig. 1(c). The irradiation interval is determined based on the spot area and coverage settings, and the coverage percentage (%) is expressed as follows.

$$\text{Coverage}(\%) = \pi D^2/4d^2 \times 100, \quad (3)$$

where "*D*" signifies the spot diameter and "*d*" denotes the irradiation interval, the latter was adjusted to achieve a coverage of approximately 700% during the experimental process. Dry laser peening was carried out both at the focal position in a linear propagation regime and the position where the spot area reached its maximum extent. To assess the peening effect, compressive residual stress profiles in the depth direction were measured. For the residual stress measurements, an X-ray residual stress measurement system (Pulstec, μ-X360s) was employed.[25] The experiment utilized a CrKα X-ray with a wavelength of 2.2897 Å, and the (311) plane was adopted for analysis. Depth residual stress measurements were conducted through successive electropolishing of the surface layer.

Figures 2(a)–2(c) illustrate the fluence distributions achieved by nonlinear propagation calculations for focused pulses at 0.1 mJ, 1.0 mJ, and 3.0 mJ, respectively. At higher pulse energy levels, nonlinear optical phenomena significantly influence the divergence of the laser beam in the upstream. The most tightly focused position was observed at approximately 0.4 mm upstream for 0.1 mJ, 2.1 mm upstream for 1.0 mJ, and 3.8 mm upstream for 3.0 mJ. The fluence distribution at these positions exhibited a transformation from a Gaussian distribution to a top-hat-like pattern, featuring peak fluences of approximately 13 J cm^{-2}, 15 J cm^{-2}, and 15 J cm^{-2}, respectively. Notably, the increase in fluence is marginal even with a tenfold rise in pulse energy, primarily leading to an expansion of the focused diameter. Consequently, precise irradiation position control that considers these laser divergences becomes indispensable.

The optical Kerr effect exhibits negligible influence upstream in the nonlinear propagation calculations, while the air ionization plays a decisive role in shaping the laser focusing characteristics. These observations correspond to the outcomes of prior research, which indicate an increase in plasma production with higher numerical aperture (NA) values,[26] and a wavelength shift limited to the blue spectrum.[27] The plasma production is contingent upon laser intensity, thereby rendering it infeasible to augment the laser intensity distribution (fluence distribution) at the focus through the utilization of high pulse laser energy. Instead, to amplify the peak fluence, one must either escalate the NA or extend the pulse duration.[28]

Figure 3 illustrates the transition of spot area in the propagation direction near the focal point for each energy. Error bars are given by the maximum and minimum measured four radius in the vertical and horizontal directions from the center of the ablation, and plots were averaged. Under the 3.0 mJ condition, the minimum error is large because debris and burrs are unevenly distributed. At 0.1 mJ, the spot region shows a relatively symmetrical shape, slightly shifting upstream of the focal point. However, at 1.0 mJ and 3.0 mJ, the ablation behind the focal point decreases, resulting in an asymmetrical spot region. In Fig. 3, the boundaries exceeding the 2.5 μm ablation threshold in the calculated fluence distribution are superimposed for comparison. The fluence threshold for best agreement was

Table I. The parameter used in Eqs. (1), and (2).

Parameter	Value
n_0: linear refraction index	1.000283
$k_0^{(2)}$: group velocity dispersion	0.2 fs^2 cm^{-1}[23]
n_2: nonlinear index coefficient	2.9×10^{-19} cm^2 W^{-1}[24]
τ_c: electron collision time	350 fs[13]
σ_{IB}: cross section for inverse Bremsstrahlung	5.5×10^{-20} cm^2

© 2023 The Author(s). Published on behalf of The Japan Society of Applied Physics by IOP Publishing Ltd

Table II. Chemical composition (wt%) of the 2024-T351 aluminum alloy.

Si	Fe	Cu	Mn	Mg	Cr	Zn	Ti	Al
0.0780	0.0970	4.5790	0.5340	1.5130	0.0010	0.0330	0.0237	Bal.

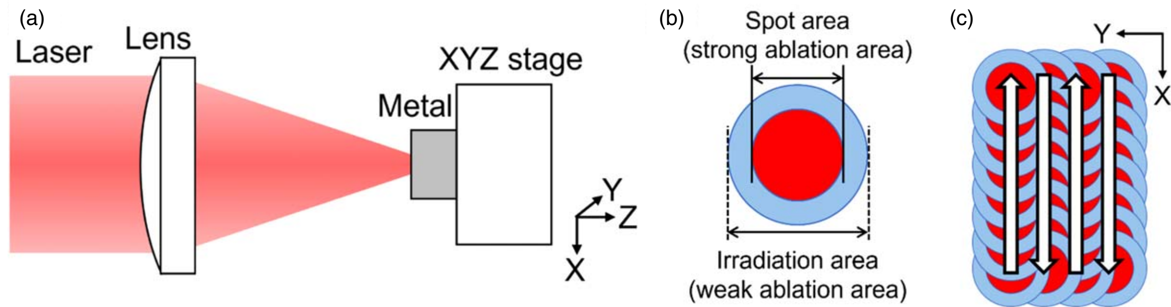

Fig. 1. Schematic illustrations of the experimental setup of dry laser peening. (a) Irradiation method of ultrashort pulse laser. (b) Laser irradiation mark. (c) Scan irradiation method of the ultrashort pulse lasers.

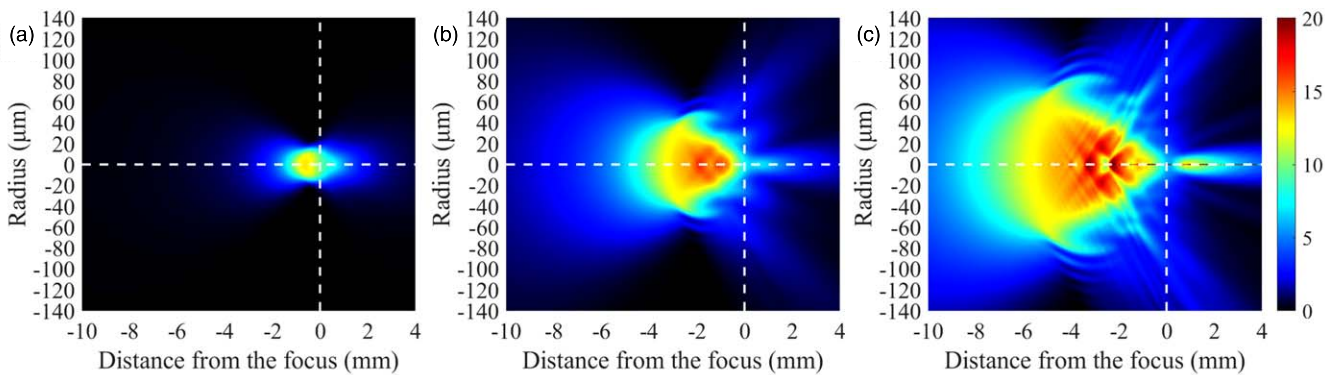

Fig. 2. Fluence distribution for each pulse energy as obtained from numerical simulation: (a) 0.1 mJ, (b) 1.0 mJ, and (c) 3.0 mJ.

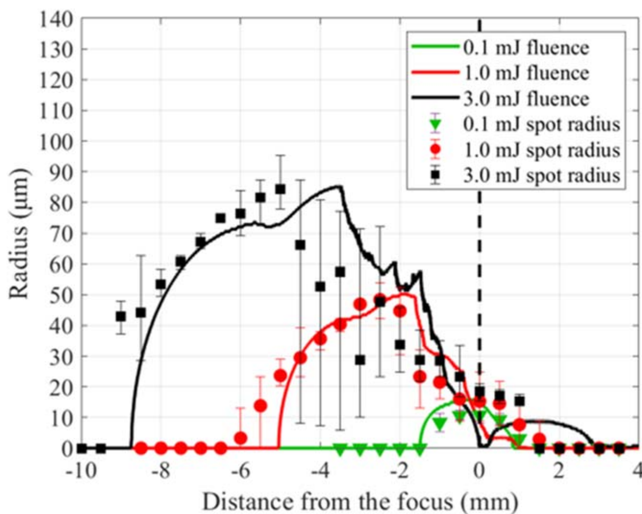

Fig. 3. Comparison of fluence thresholds from numerical simulation and the transition of spot area in the direction of propagation results.

6.5 J cm^{-2}. The transition of spot area is quantitatively represented for all energy conditions except at the focal point, confirming the reliability of the calculation results. The expanded spot range at the focal point, exceeding the calculated values for the 1.0 and 3.0 mJ conditions, can be attributed to the pre- and post-pulses of this laser system. The maximum ablation depth per 8 pulses at the most focused position remains constant at 5 μm ± 1 μm. This consistency reflects the calculation result, indicating that the peak fluence at the most focused position remains approximately constant with an increase in pulse energy. These findings demonstrate the excellent agreement between the ultrashort pulse laser focusing characteristics at several mJ pulse energies and general nonlinear propagation calculations.

Figure 4(a) depicts the peening outcomes at the focal position in a linear propagation regime and the most focused position under 1.0 mJ conditions. At the focal position in a linear propagation regime, the compressive residual stress is small, while at the most focused position, a compressive residual stress of approximately 0.2% proof stress can be achieved. 0.2% proof stress is the stress at 0.2% permanent strain and used in the same sense as yield stress. Residual stress, being an elastic property, is typically confined within this range. Therefore, the introduction of a compressive residual stress of this magnitude implies a substantial peening effect. Thus, precise control of the irradiation position plays a pivotal role in achieving the most effective peening results, especially under high-energy conditions where significant focusing characteristics changes.

Figure 4(b) presents the peening outcomes at the most focused position for each energy level. The spot diameters D at the peening process positions were 35 μm, 110 μm, and 160 μm for pulse energies of 0.1 mJ, 1.0 mJ, and 3.0 mJ, respectively. The corresponding irradiation intervals d were 12 μm, 32 μm, and 48 μm. The total energy input to the machining surface remains nearly equal. Under all

© 2023 The Author(s). Published on behalf of The Japan Society of Applied Physics by IOP Publishing Ltd

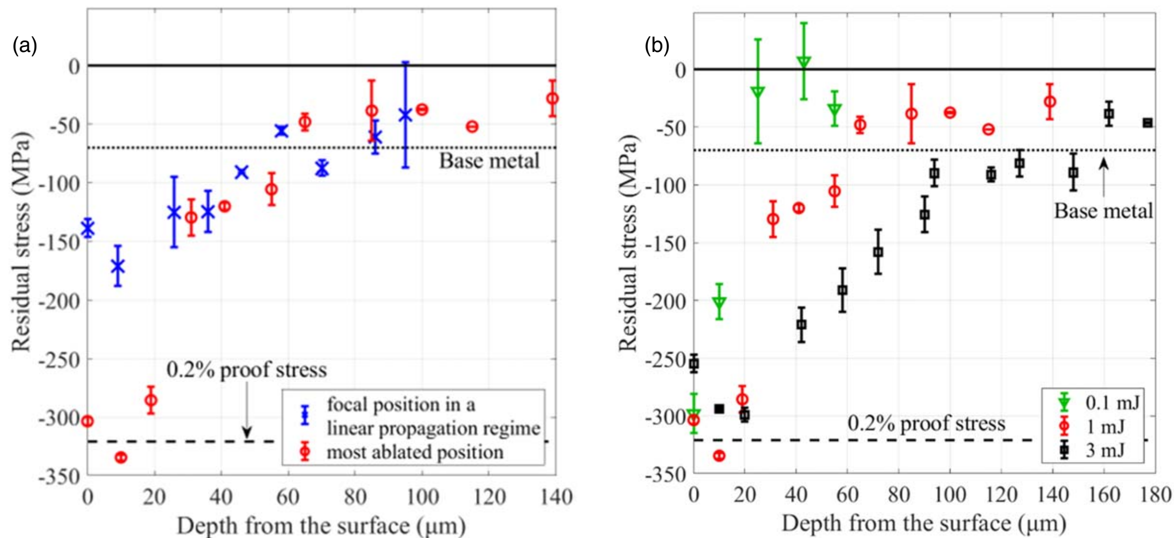

Fig. 4. Depth profile of compressive residual stress after peening. (a) Variation due to irradiation position at 1.0 mJ. (b) Peening results at the optimal position for each energy level.

conditions, a compressive residual stress of approximately 0.2% proof stress was effectively induced in the surface layer. Moreover, as the pulse energy increased, the region of compressive residual stress application became noticeably deeper. The increase in pulse energy, influenced by nonlinear optical effects, does not result in an increase in fluence but leads to an expansion of the spot diameter. As such, it can be demonstrated that the peening effect depth is determined by the spot diameter. Dry laser peening is occasionally perceived as having a shallow depth of compressive residual stress application due to its short pulse duration, yet in actuality, this is attributed to the constraints in pulse energy and the small spot diameter.[8)] A correlation between the depth of effect induced by femtosecond laser processing and the spot diameter has also been suggested in Ref. 29. This is attributed to the pressure reduction resulting from the geometric effects of the shock wave and the dissipation of shock pressure through reflected and edge waves.[30)] Dry laser peening can be anticipated to yield effects at an even greater depth by employing higher pulse energies and precise irradiation position control.

In conclusion, this study comprehensively assessed the energy-dependent transition of spot area through both experimental and computational means, demonstrating quantitative consistency in the high-energy region's laser focusing characteristics. Nonlinear optical phenomena in the air lead to substantial laser divergence on the upstream side during ultrashort laser pulse focusing at high energies. Augmenting the pulse energy does not result in an increase in the fluence at the most focused point, instead leading to a top-hat-like distribution. Processing at the focal point is unsuitable for high pulse energy ultrashort pulse laser processing, emphasizing the crucial requirement for precise control of the irradiation position. By applying the knowledge acquired in this investigation to dry laser peening, it becomes feasible to perform appropriate processing and enhance the peening effect, even in scenarios characterized by pronounced laser divergence at high pulse laser energies. Visualization of fluence distribution demonstrates that the depth of the peening effect is constrained by the spot diameter, and processing at even higher pulse energies is expected. In essence, visualizing the laser focusing characteristics through numerical simulation paves the way for precise control, thus contributing to the advancement of laser processing techniques.

Acknowledgments This work was supported in part by Ministry of Education, Culture, Sports, Science and Technology (MEXT) - Quantum Leap Flagship Program (MEXT Q-LEAP) Grant No. JPMXS0118068348, and JSPS KAKENHI Grant No. 22J10847.

ORCID iDs Itsuki Nishibata https://orcid.org/0000-0001-8605-8657
Tomokazu Sano https://orcid.org/0000-0003-2624-5092

1) B. N. Chichkov, C. Momma, S. Nolte, F. von Alvensleben, and A. Tünnermann, Appl. Phys. A **63**, 109 (1996).
2) S. Nolte, C. Momma, H. Jacobs, A. Tünnermann, B. N. Chichkov, B. Wellegehausen, and H. Welling, J. Opt. Soc. Am. B **14**, 2716 (1997).
3) R. Evans et al., Phys. Rev. Lett. **77**, 3359 (1996).
4) T. Sano et al., J. Laser Appl. **29**, 012005 (2017).
5) R. Fabbro, P. Peyre, L. Berthe, and X. Sherpereel, J. Laser Appl. **10**, 265 (1998).
6) Y. Sano, M. Obata, T. Kubo, N. Mukai, M. Yoda, K. Masaki, and Y. Ochi, Mater. Sci. Eng. A **417**, 334 (2006).
7) M. A. Kattoura, S. C. Bovid, D. F. Lahrman, and A. H. Clauer, *Shot Peening—A Dynamic Application and its Future* (Metal Finishing News, Wetzikon, 2021) ed. 6th, Chap. 14.
8) P. Chessa, E. De Wispelaere, F. Dorchies, V. Malka, J. R. Marquès, G. Hamoniauxs, P. Mora, and F. Amiranoff, Phys. Rev. Lett. **82**, 552 (1999).
9) K. Ishikawa, H. Kumagai, and K. Midorikawa, Phys. Rev. E **66**, 056608 (2002).
10) X. Zhao and Y. C. Shin, Appl. Sur. Sci. **283**, 94 (2013).
11) C. Pasquier, M. Sentis, O. Utéza, and N. Sanner, Appl. Phys. Lett. **109**, 051102 (2016).
12) L. Bergé, S. Skupin, R. Nuter, J. Kasparian, and J.-P. Wolf, Rep. Prog. Phys. **70**, 1633 (2007).
13) A. Couairon and A. Mysyrowicz, Phys. Rep. **441**, 47 (2007).
14) S. L. Chin et al., Laser Phys. **22**, 1 (2012).
15) J. Sun and J. P. Longtin, J. Opt. Soc. Am. B **21**, 1081 (2004).
16) S. R. Vatsya, C. Li, and S. K. Nikumb, J. Appl. Phys. **97**, 034912 (2005).
17) C. Li, S. R. Vatsya, and S. K. Nikumb, J. Laser Appl. **19**, 26 (2007).
18) R. Yamada, W. Komatsubara, H. Sakurai, K. Konishi, N. Mio, J. Yumoto, and M. Kuwata-Gonokami, Opt. Express **31**, 7363 (2023).
19) A. Schmitt-Sody, H. G. Kurz, L. Bergé, S. Skupin, and P. Polynkin, New J. Phys. **18**, 093005 (2016).
20) J. K. Koga et al., J. Phys. D: Appl. Phys. **43**, 025204 (2010).
21) A. M. Perelomov, V. S. Popov, and M. V. Terent'ev, Sov. Phys. JETP **23**, 924 (1966).

© 2023 The Author(s). Published on behalf of The Japan Society of Applied Physics by IOP Publishing Ltd

22) A. Talebpour, J. Yang, and S. L. Chin, Opt. Commun. **163**, 29 (1999).
23) P. J. Wrzesinski, D. Pestov, V. V. Lozovoy, J. R. Gord, M. Dantus, and S. Roy, Opt. Express **19**, 5163 (2011).
24) E. T. J. Nibbering, G. Grillon, M. A. Franco, B. S. Prade, and A. Mysyrowicz, J. Opt. Soc. Am. B **14**, 650 (1997).
25) K. Tanaka, Mech. Eng. Rev. **6**, 18 (2019).
26) F. Théberge, W. Liu, P. Tr. Simard, A. Becker, and S. L. Chin, Phys. Rev. E **74**, 036406 (2006).
27) Y. E. Geints, D. V. Mokrousova, D. V. Pushkarev, G. E. Rizaev, L. V. Seleznev, I. Y. Geints, A. A. Ionin, and A. A. Zemlyanov, Opt. Laser Technol. **143**, 107377 (2021).
28) I. Nishibata, N. Nakanii, and T. Sano, Opt. Commun. **2**, 1735 (2023).
29) H. Nakano, S. Miyauti, N. Butani, T. Shibayanagi, M. Tsukamoto, and N. Abe, J. Laser Micro Nanoeng. **4**, 35 (2009).
30) S. Nakazawa, S. Watanabe, Y. Iijima, and M. Kato, Icarus **156**, 539 (2002).

© 2023 The Author(s). Published on behalf of The Japan Society of Applied Physics by IOP Publishing Ltd